Supplement of Biogeosciences, 21, 2795–2809, 2024
https://doi.org/10.5194/bg-21-2795-2024-supplement

Biogeosciences Open Access EGU

Supplement of

The optimum fire window: applying the fire–productivity hypothesis to Jurassic climate states

Teuntje P. Hollaar et al.

Correspondence to: Teuntje P. Hollaar (t.p.hollaar@uu.nl)

Table S1: Overview of the number of samples studied per proxy for SPB and LPE intervals of the Mochras borehole.

Proxies	**LPE**	**SPB**
Macrocharcoal	204	54
Microcharcoal	200	54
Palynofacies	162	42
Mass spectrometry	193	50
Clay mineralogy	194	55

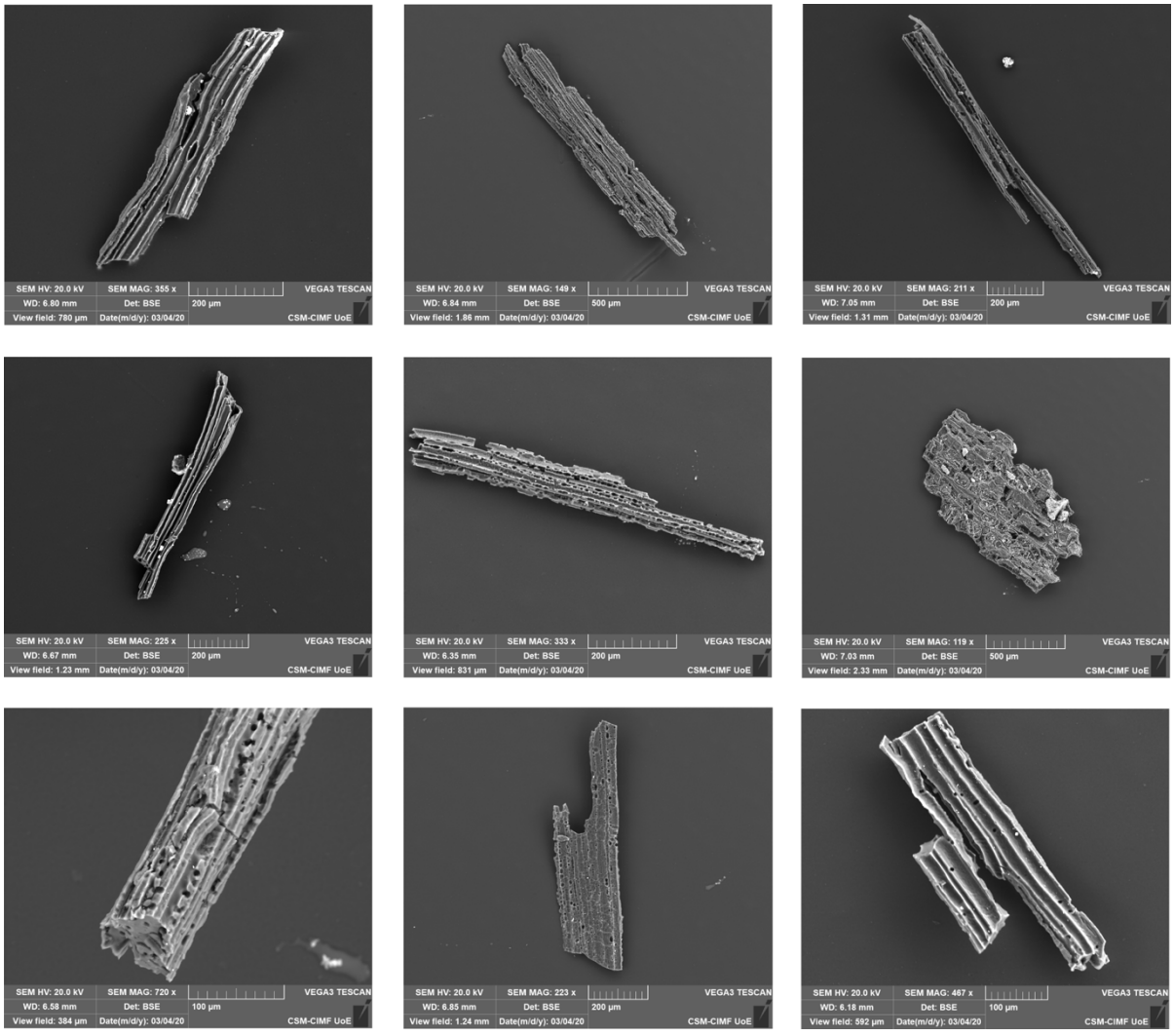

Figure S1: Scanning Electron Microscope (SEM) images of Pliensbachian charcoal particles of the Mochras borehole. These charcoal particles from the studied interval of the Mochras borehole show cellular structure, tracheids, bordering pits and rays.

Table S2: Charcoal identification table.

Identification characteristics	Charcoal	Non-charcoalified
Colour	Opaque, black, silver	Brown, orange edges
Shine	Reflective, lustrous	Dull
Structure	Original anatomy preserved, cellular structure visible	No apparent structure
Shape	Elongated, sharp edges	Rounded, paper thin
Fracture	Brittle, splintery fragmentation	Conchoidal, total disintegration, orange appearance

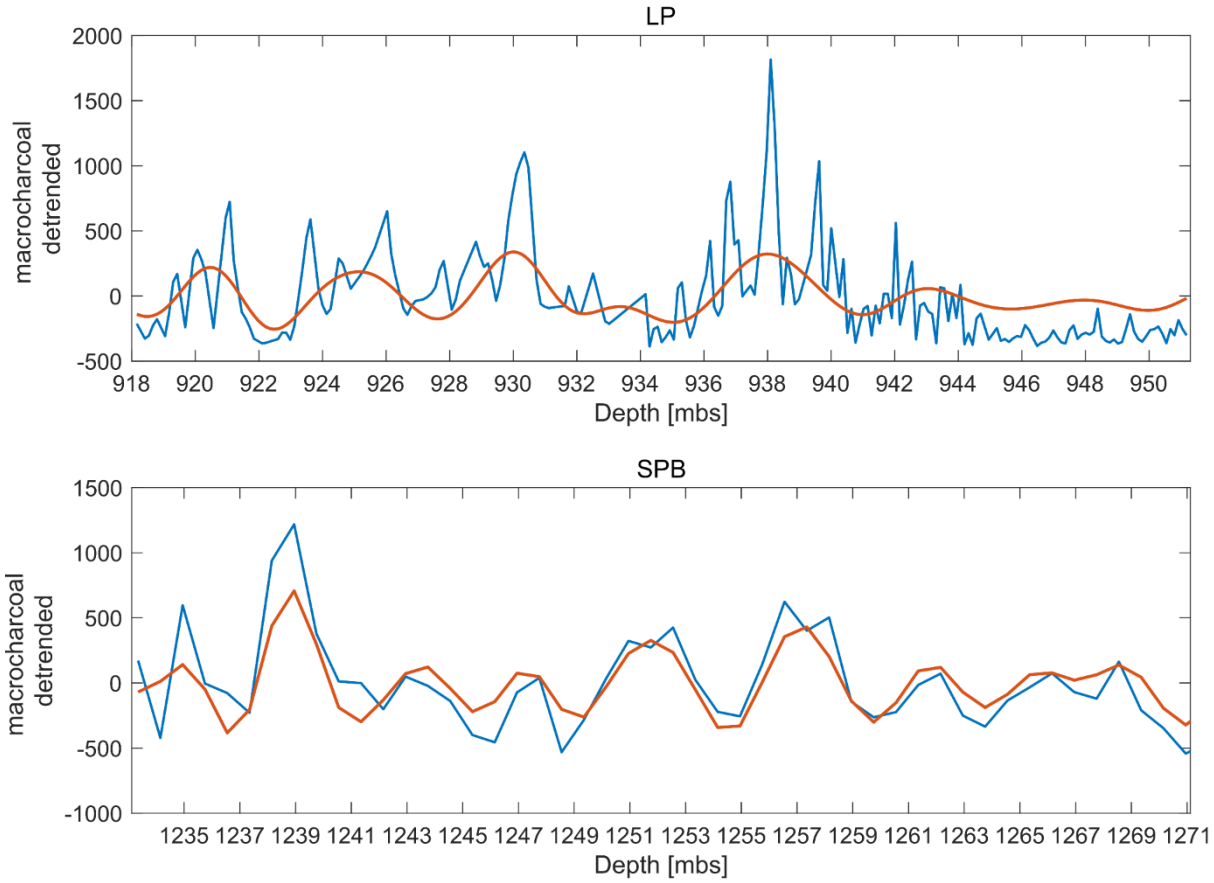

Figure S2: Macrocharcoal and the 10.2 – 3.2 m filter. (a) The macrocharcoal record (blue) of the LPE interval is linear detrended and the 10.2 – 3.2 m period is filtered out of the macrocharcoal record in

Acycle. This filter represents the 100 kyr periodicity in the depth domain (Ruhl et al., 2016). The number of peaks corresponds to the number of short eccentricity cycles in the studied interval found by Ruhl et al. (2016) and do capture the ~5 m bundles observed in the macrocharcoal record. (b) The macrocharcoal record of the SPB is linear detrended (blue). The 10.2 – 3.2 m signal (orange) is filtered from the macrocharcoal record. The individual peaks capture the ~5 m peaks in macrocharcoal observed in this record. Also, nine peaks are observed, which is in agreement with Ruhl et al. (2016) who found nine 100 kyr eccentricity cycles for the same interval.

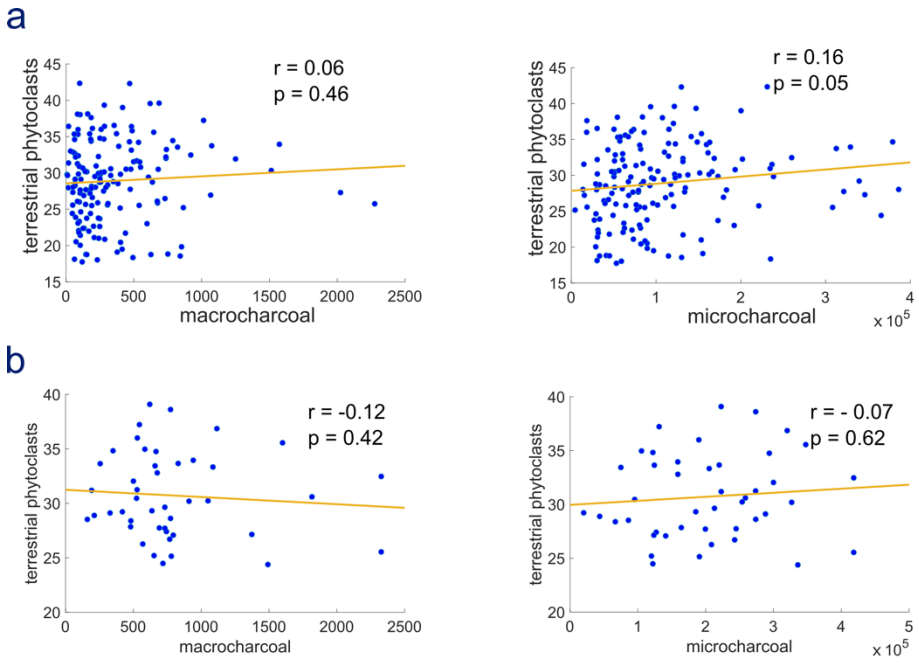

Figure S3: Scatter plots indicate no correlation between the percentage of terrestrial phytoclasts and micro- and macro-charcoal abundance. (a) Shows the data for the LPE interval. No significant correlation (Pearson's correlation) was found between the abundance of macrocharcoal and terrestrial phytoclasts. A very weak significant correlation was found between the abundance of microcharcoal and terrestrial phytoclasts. (b) Shows the data for the SPB interval. No significant correlation was found between the abundance of macro- and micro-charcoal with the percentage of terrestrial phytoclasts.

Table S3: Summary statistics charcoal abundance for the LPE and the SPB interval.

Summary statistics	**LPE**		**SPB**	
	Macrocharcoal	Microcharcoal	Macrocharcoal	Microcharcoal
Mean	376	$1.1x10^5$	787	$2x10^5$
Min	8	$4.5x10^3$	99	$2x10^4$
Max	2276	$4.3x10^5$	2327	$4.2x10^5$

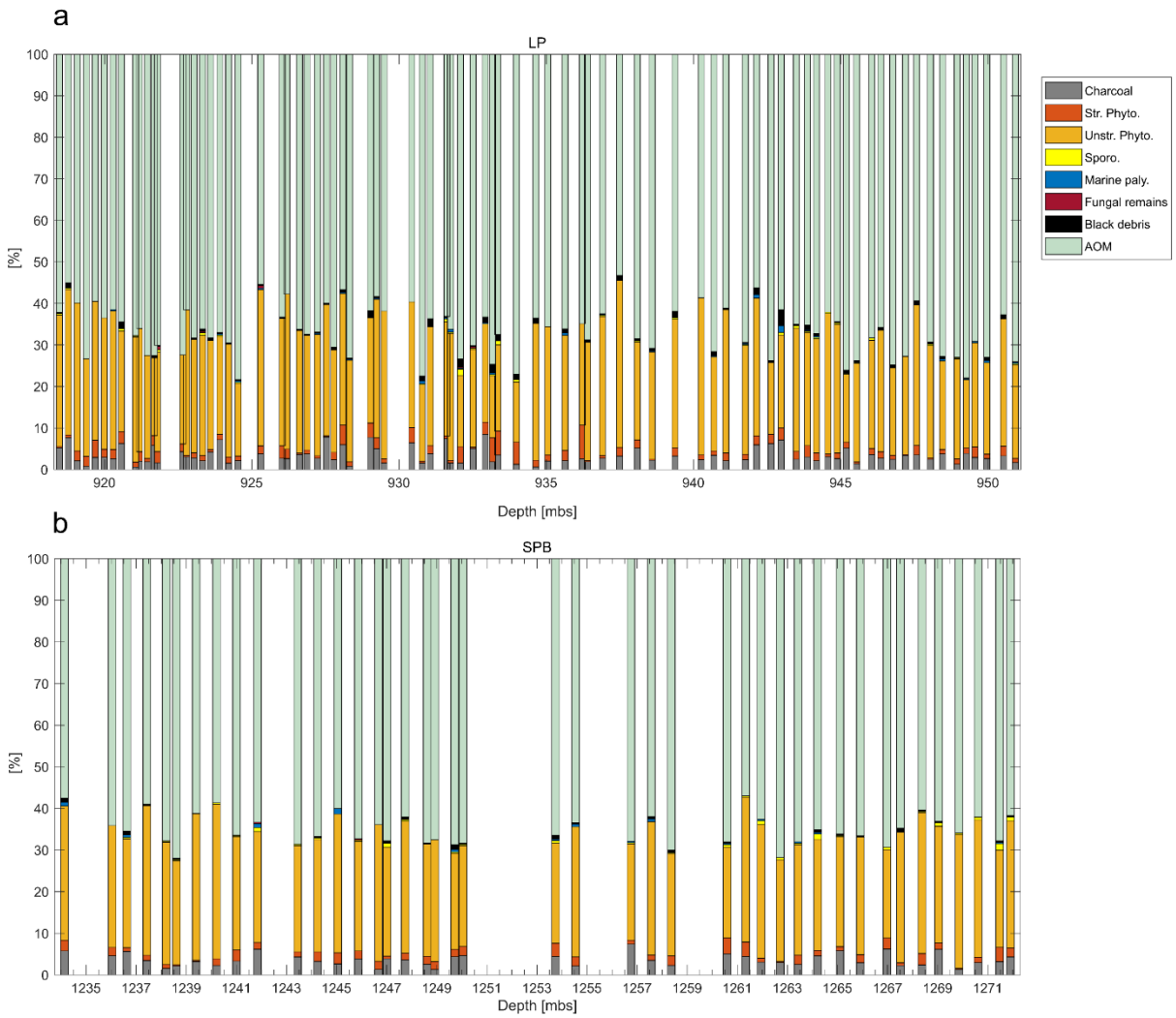

Figure S4: Palynofacies of the (a) LP (published in Hollaar et al. (2021; 2023)) and (b) SPB studied intervals of the Mochras borehole. Relative abundance of the organic particle type identified under the reflective microscope. In each sample >300 organic particles were identified and grouped based on Oboh-Ikuenobe et al. (2005). Amorphous Organic Matter (AOM) is >50 % in all samples and constitutes the main bulk of the marine derived organic matter. This is followed by the group unstructured phytoclasts, which is of terrestrial origin. Only minor changes are observed in the

relative abundance of terrestrial vs marine particulate organic matter and no abrupt or large shifts are observed. In this deep-time fire study, the palynofacies are a proxy for potential abrupt changes in sedimentation rate, terrestrial run-off into the marine environment or organic matter preservation, of which there is no evidence.

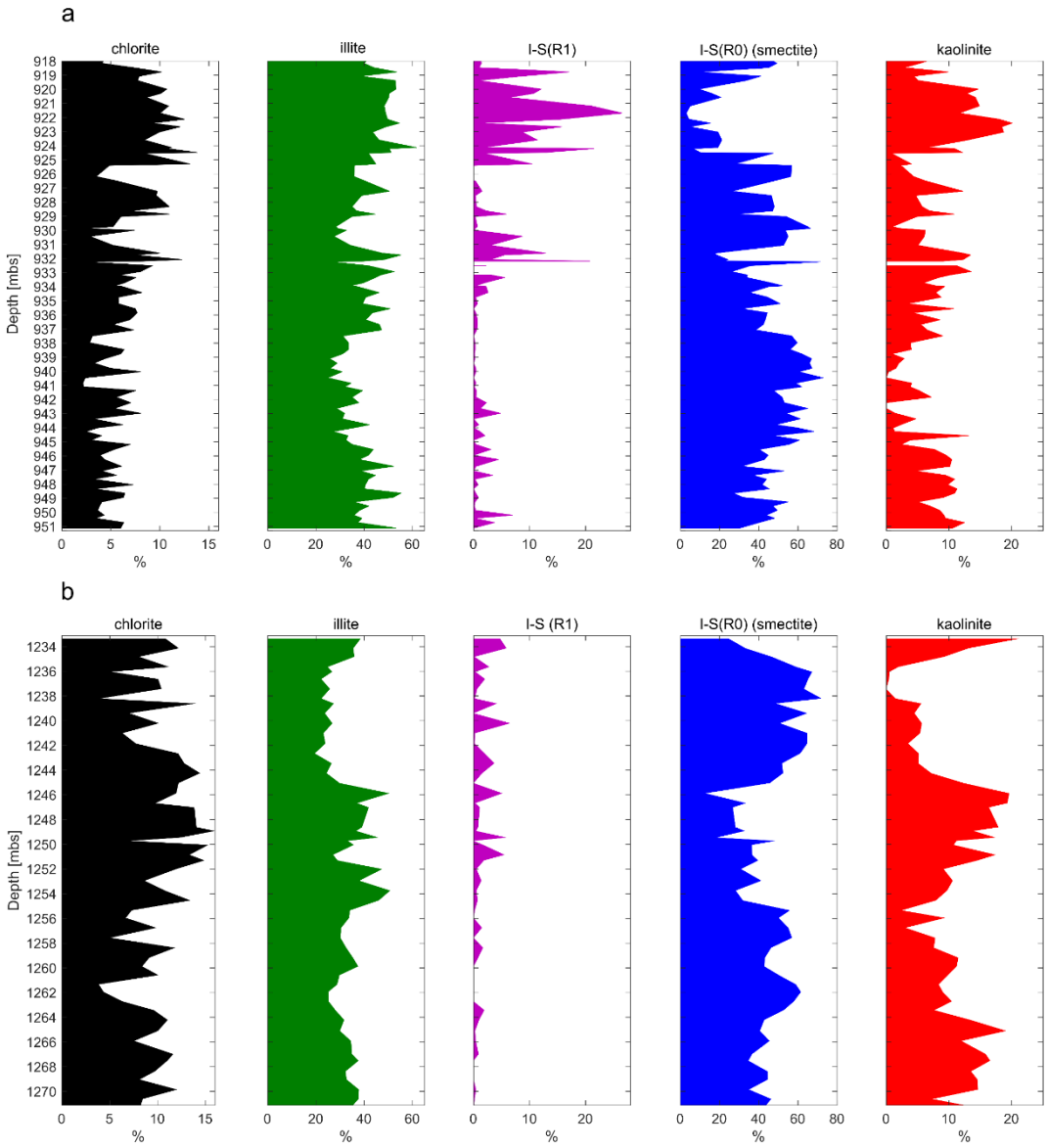

Figure S5: Clay mineralogical abundance from the sediments of the LP and the SPB in the Mochras borehole. (a) The proportions of chlorite and illite-smectite mixed layers type R1 increase to the top of the record, coeval with illite and kaolinite. A long term opposite trend is observed in the abundance of smectite and kaolinite, in which kaolinite and illite co-vary (similar of the longer Pliensbachian clay

mineralogy record of Mochras published in Deconinck et al. (2019). This indicates a climatic origin of the clay minerals (Deconinck et al., 2019) (results published in Hollaar et al. (2021; 2023)). (b) The clay mineralogical abundance record of the SPB studied interval. Chlorite is more abundant compared to the LP record. Smectite and kaolinite vary in parallel, however, the covariation of illite and kaolinite is less clear. I-S R1 type illite-smectite mixed layers are below the level of error detection (5 %) and are dismissed for interpretation in this record.

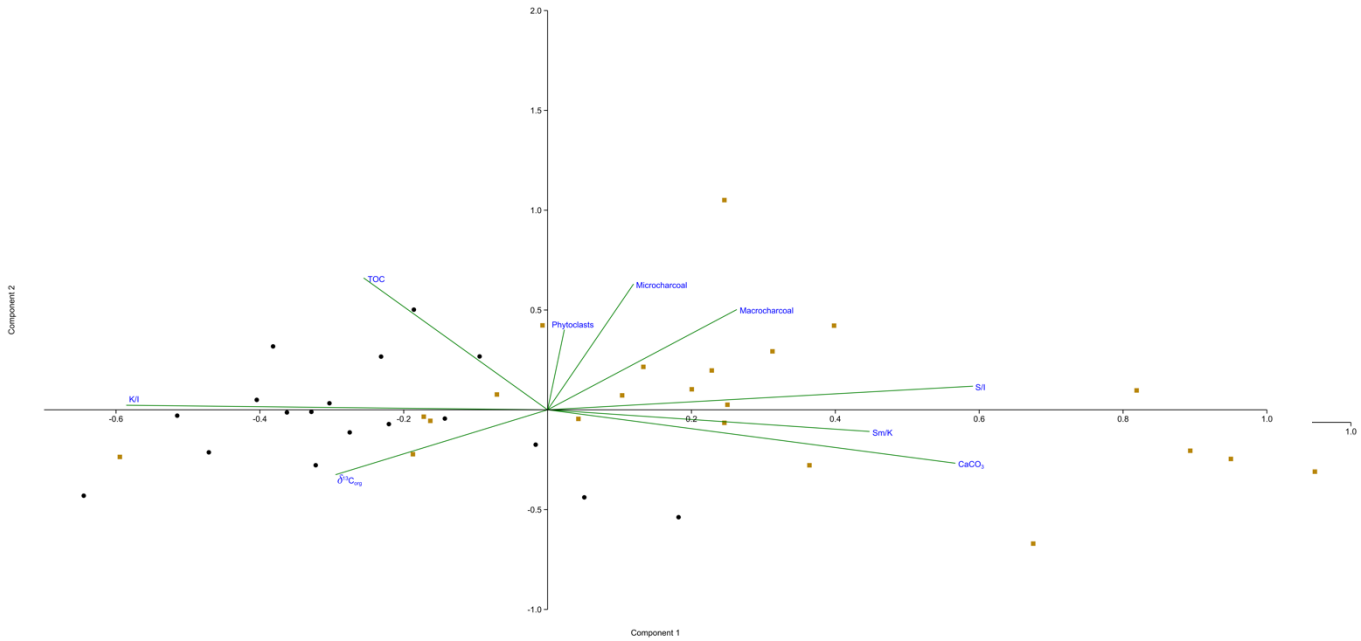

Figure S6: PCA axis cross plot of PC1 and PC2 of the SPB interval. PCA analysis indicates that PC1 has an eigenvalue of 2.68 and explains 33.6% of the variance and PC2 has an eigenvalue of 1.88 and explains 23.6% of the variance. In total PC1-2 explain 57.2% of the variance. Charcoal (macro and micro) fall to the right part of the x-axis together with S/I and Sm/K, and in opposition of K/I. This confirms the corresponding increases of smectite and charcoal during phases of maximum eccentricity. The samples from the inferred eccentricity maxima are marked by brown squares and the samples from the inferred eccentricity minima are marked by black dots.

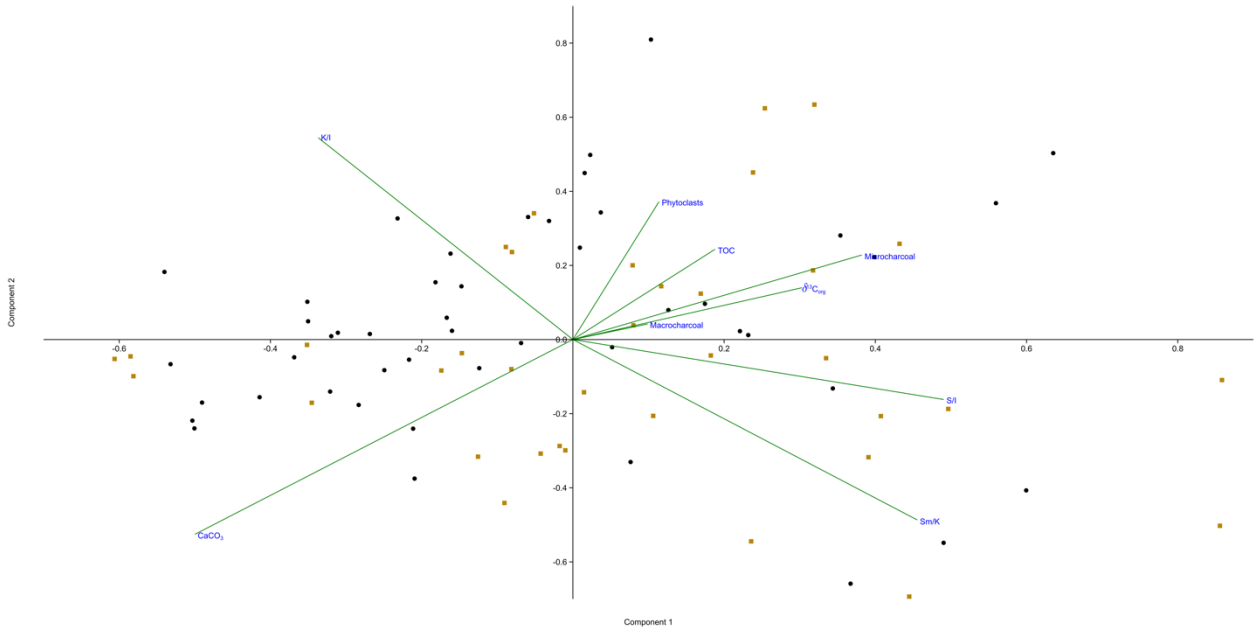

Figure S7: PCA axis cross plot of PC1 and PC2 of the LPE interval. PCA analysis indicates that PC1 has an eigenvalue of 0.11 and explains 29.9% of the variance and PC2 has an eigenvalue of 0.09 and explains 23% of the variance. In total PC1-2 explain 52.9% of the variance. The low eigenvalues for PC1 and PC2 suggest that the variance of the data is not well explained by the PC axes. However, a similar pattern is observed as in SI Fig. 6 of the SPB interval, where both charcoal size fractions and the S/I and Sm/K fall to the right of the x-axis and are in opposition of K/I (similar as in the SPB interval). This indicates an increase hydrological cycle (K/I) corresponding to minimum charcoal abundance and a slower hydrological cycle, with an annual arid season (S/I and Sm/K) leading to higher charcoal abundance. Different, however, is that TOC, terrestrial phytoclasts and $\delta^{13}C_{org}$ are also plotting to the right of the x-axis. This difference might be explained by the positive carbon-isotope excursion marking the onset of the LPE (at 930 mbs), which coincides with a short-lived peak in TOC, charcoal, smectite and terrestrial phytoclasts (see Hollaar et al., 2023). The samples from the inferred eccentricity maxima are marked by brown squares and the samples from the inferred eccentricity minima are marked by black dots.

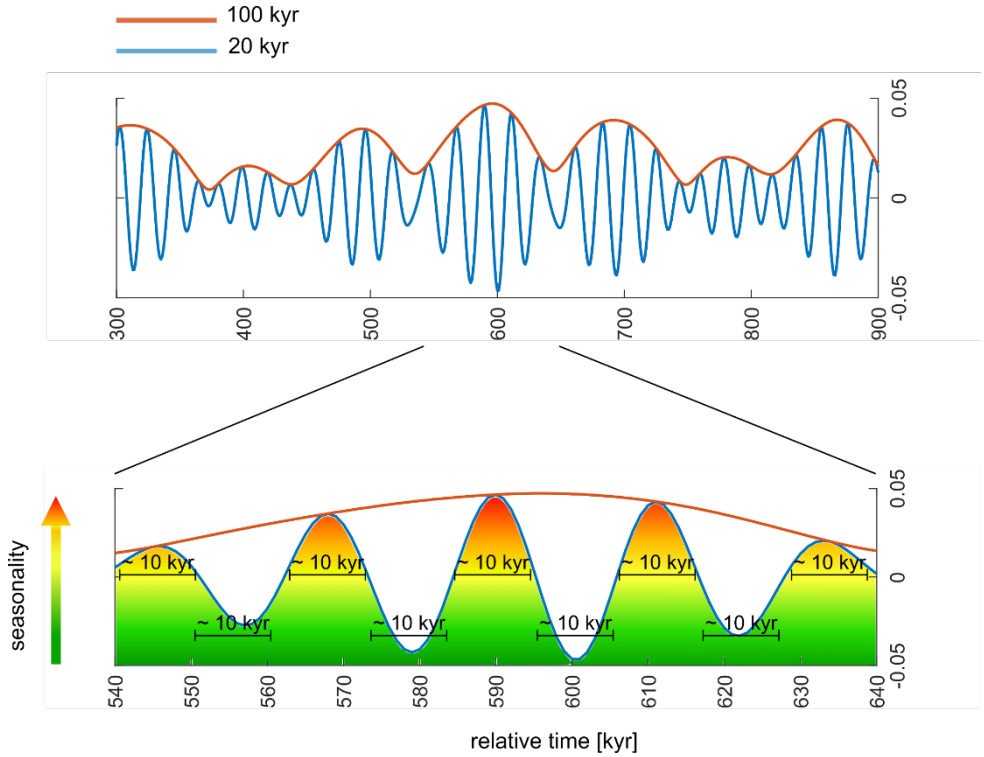

Figure S8: Schematic image showing eccentricity modulation of the precession cycle, each precession cycle contains ~ 10 kyr of minimum precessional forcing (equitable climate) and ~10 kyr of maximum precessional forcing (extreme seasonal contrast). The ~20 kyr precession and ~100 kyr eccentricity sine curves are derived from Laskar 2010d plotted in Acycle.